Open Access Full Text Article

ORIGINAL RESEARCH

High Strength and Shape Memory Spinal Fusion Device for Minimally Invasive Interbody Fusions

Min Liu[1,2], Bo Liu[2], Ziyang Liu[3], Zhen Yang[2], Thomas J Webster [4], Huan Zhou[2], Lei Yang [2]

[1]School of Materials Science and Engineering, Hebei University of Technology, Tianjin, People's Republic of China; [2]Center for Health Science and Engineering, Hebei Key Laboratory of Biomaterials and Smart Theranostics, School of Health Sciences and Biomedical Engineering, Hebei University of Technology, Tianjin, 300131, People's Republic of China; [3]Department of Orthopedics, Tianjin Hospital, Tianjin, People's Republic of China; [4]School of Engineering, Saveetha University, Chennai, India

Correspondence: Huan Zhou; Lei Yang, Center for Health Science and Engineering, School of Health Sciences and Biomedical Engineering, Hebei University of Technology, Tianjin, 300131, People's Republic of China, Email zhouhuan@hebut.edu.cn; ylei@hebut.edu.cn

Introduction: Lumbar interbody fusion is widely employed for both acute and chronic spinal diseases interventions. However, large incision created during interbody cage implantation may adversely impair spinal tissue and influence postoperative recovery. The aim of this study was to design a shape memory interbody fusion device suitable for small incision implantation.

Methods: In this study, we designed and fabricated an intervertebral fusion cage that utilizes near-infrared (NIR) light-responsive shape memory characteristics. This cage was composed of bisphenol A diglycidyl ether, polyether amine D-230, decylamine and iron oxide nanoparticles. A self-hardening calcium phosphate-starch cement (CSC) was injected internally through the injection channel of the cage for healing outcome improvement.

Results: The size of the interbody cage is reduced from 22 mm to 8.8 mm to minimize the incision size. Subsequent NIR light irradiation prompted a swift recovery of the cage shape within 5 min at the lesion site. The biocompatibility of the shape memory composite was validated through in vitro MC3T3-E1 cell (osteoblast-like cells) adhesion and proliferation assays and subcutaneous implantation experiments in rats. CSC was injected into the cage, and the relevant results revealed that CSC is uniformly dispersed within the internal space, along with the cage compressive strength increasing from 12 to 20 MPa.

Conclusion: The results from this study thus demonstrated that this integrated approach of using a minimally invasive NIR shape memory spinal fusion cage with CSC has potential for lumbar interbody fusion.

Keywords: shape memory, interbody fusion cage, NIR responsive, calcium phosphate cement, minimally invasive

Introduction

Fusion surgery is commonly applied as an attempt to alleviate pain and stabilize symptomatic spinal segments. The procedure typically involves inserting an implant, known as a "cage", into the disc space between two vertebrae to stabilize the spine until the bone grows together to achieve interbody fusion. Annually, approximately 210,000 fusions are performed in the United States, with an escalating trend attributed to population aging, lifestyle changes, and other factors.[1] However, current approaches have led to spinal fusion failure rates as high as 35% with an average of 25% of patients requiring another spinal case after just 10–20 years.[2]

Over the recent decades, titanium (Ti) and poly-ether-ether-ketone (PEEK) are acknowledged as the primary fusion materials for cage fabrication. In spite of their impressive track record in medical practice, several key limitations of cages are now documented in clinical reports. For example, the mismatched elastic modulus between Ti and vertebra can cause stress shielding, leading to intervertebral settlement and space collapse. Moreover, the surgical implantation required for cage placement between adjacent vertebrae leads to spinal tissue defects and associated risks. This procedure often triggers significant bleeding, with studies reporting transfusion rates of 50–81% for adult spinal fusions, elevating the risk for transfusion reactions, alloimmunization, and infection.[3,4] Surgical-induced tissue defects further complicate postoperative recovery, prolonging hospital stays. Therefore, development of fusion cages adaptable to vertebra

mechanical properties and applicable to smaller surgical incision becomes imperative to avert post-surgery complications and expedite patient recovery.

Shape memory polymers (SMPs) are a class of programmable smart materials that can change between permanent and temporary shapes.[5] Once the permanent shape is established, altering the conditions (typically based on temperature) to exceed the glass transition temperature (T_g) or the glass melting temperature (T_m) enables shaping under mechanical forces to achieve a desired temporary shape. The fixation of the temporary shape can be obtained through subsequent cooling below T_g or T_m. When stimuli (such as heat, light, or other triggering solvents) to switch upon transformation are reapplied, the permanent shape can be recovered.[5–7]

Since 2002, SMPs have been attempted in medical practice, with typical examples including surgical sutures[8,9] and porous scaffolds.[10] The potential of SMPs for minimally invasive surgery has also been identified by their ability to be programmed into compact, small-sized temporary shapes that are suitable for small-channel incisions and delivery, and are subsequently restored to their original shape by a predetermined stimulus to achieve a specific function.[11–13] To achieve remote timing control of the shape memory function, responsive agents are introduced in order to synthesize shape memory polymer composites (SMPC).[14] Examples of these responsive substances include graphene, black phosphorus, polydopamine, carbon nanomaterials, and iron tetraoxide nanoparticles.[15–21] Back in 2019, our group and collaborators also reported near-infrared (NIR) light-responsive shape memory composites (LSMPCs) as a proof-of-concept 4D printed brain model, providing a dynamic platform for modulating neural stem cell behaviors.[22]

Regarding the benefits of SMPC and the necessity to minimize the surgical incision as much as possible to reduce spinal tissue defect and shorten post-surgery recovery, development of a shape memory intervertebral fusion cage utilizing NIR light-responsive shape memory composites (Cage-LSMPC) were created for the first time in the current work.

In addition to the cage, bone regenerative grafts from the iliac crest site are sometimes clinically used as a filler to enhance bony fusion, owing to their enhanced effect on natural bone morphogenetic protein (BMP) and other factors favoring the success of bone grafts.[23] However, grafted bone from the iliac crest site results in as much as a 50% morbidity rate at the donor site.[24] In spite of that, synthetic grafts with BMP-2 are developed as an alternative to enhance bone growth. However, serious complications (such as implant displacement, subsidence, infection, low sperm count, radiculitis, ectopic bone formation, and osteolysis) have been reported from such products.[25]

Previously, we have studied a load-bearing calcium phosphate-starch cement (CSC) for vertebroplasty, which is an injectable and self-hardening multi-phase calcium phosphate nanocomposite constructed by the self-assembly of calcium phosphate and starch nano-networks.[26] The CSC addresses issues of bioactivity, degradability, and exothermic damage to tissues in the current orthopedic clinically used polymethylmethacrylate (PMMA) bone cements. The homogeneous dispersion ability and bone-matched mechanical properties suggest that injectable CSC can be a promising replacement for bone grafts used in conjunction with fusion devices.

Considering all of the above, herein, we developed a novel split-type spinal fusion device that combines a NIR-responsive shape memory polymer cage and an injectable CSC filler. Relying on the temperature-sensitive shape memory endowed by the SMPs, a fusion cage of 22 mm width was manipulated into a temporary insertion shape of 8.8 mm width. After NIR irradiation, the cage recovered to its initial shape within 5 min. Subsequently, CSC was injected into the cage through the pre-designated injection channel, acting as a reinforcement agent model to improve the compressive strength of the cage as well as accelerate the bony fusion. Overall, this integrated spinal fusion device provides potential in minimally invasive spinal surgery.

Experiment
Materials
Bisphenol A diglycidyl ether and decylamine were purchased from Macklin Reagent (China). Polyether amine D-230 was purchased from Rhawn (China). A Cell Count Kit-8 (CCK-8) and Live/dead cell double staining kit were bought from Beyotime Biotechnology (China). $BaSO_4$ was purchased by Qingdao Red Butterfly Precision Material Co., Ltd of China. Waxy starch (WS) was provided by Qinhuangdao Lihua Starch Co., Ltd of China. α-tricalcium phosphate (α-TCP) was obtained from Suzhou Dingan Technology Co., Ltd of China. Dicalcium phosphate dehydrate ($CaHPO_4 \cdot 2H_2O$) was

purchased from Spectrum Chemical Manufacturing Corp-China (China). Penicillin–streptomycin mixture, fetal bovine serum and α-MEM were purchased from Gibco Life Technology (USA). Fe_3O_4 and other chemicals were purchased from Aladdin Chemicals (China) as received.

Synthesis of SMPs and LSMPC

The SMPs were synthesized by combining 1 mL of bisphenol A diglycidyl ether, 122 μL of polyether amine D-230, and 500 μL of decylamine at 50 °C with stirring for 10 min (Figure 1a). The resulting mixture was then poured into a 3D printed mold and cured at 40 °C for 2 h in ambient conditions. The curing process was then continued by baking at 70 °C for 48 h. The molecular structure of the resulted SMP is shown in Figure 1b.

To prepare LSMPC, the solution for SMPs was stirred for 5 min at 50 °C. Then, 0.0052g, 0.0087g, or 0.014g of Fe_3O_4 with photothermal capability were added to the solution, respectively. This mixture was ultrasonicated for 1 min and mechanically stirred for 5 min. The added Fe_3O_4 mass accounted for 0.3%, 0.5% and 0.8% of the as-formed composite, and the resulting samples were referred to as LSMPC-0.3, LSMPC-0.5, LSMPC-0.8, respectively.

Characterization and Evaluation

Photothermal Characteristic Tests

A near-infrared (NIR) laser (Changchun New Industry Optoelectronics Co., Ltd., China) was used to test the NIR induced photothermal effect on the samples. A power of 1 W was used to irradiate the specimen at a distance of 20 cm, and the temperature was recorded at intervals of 20s.
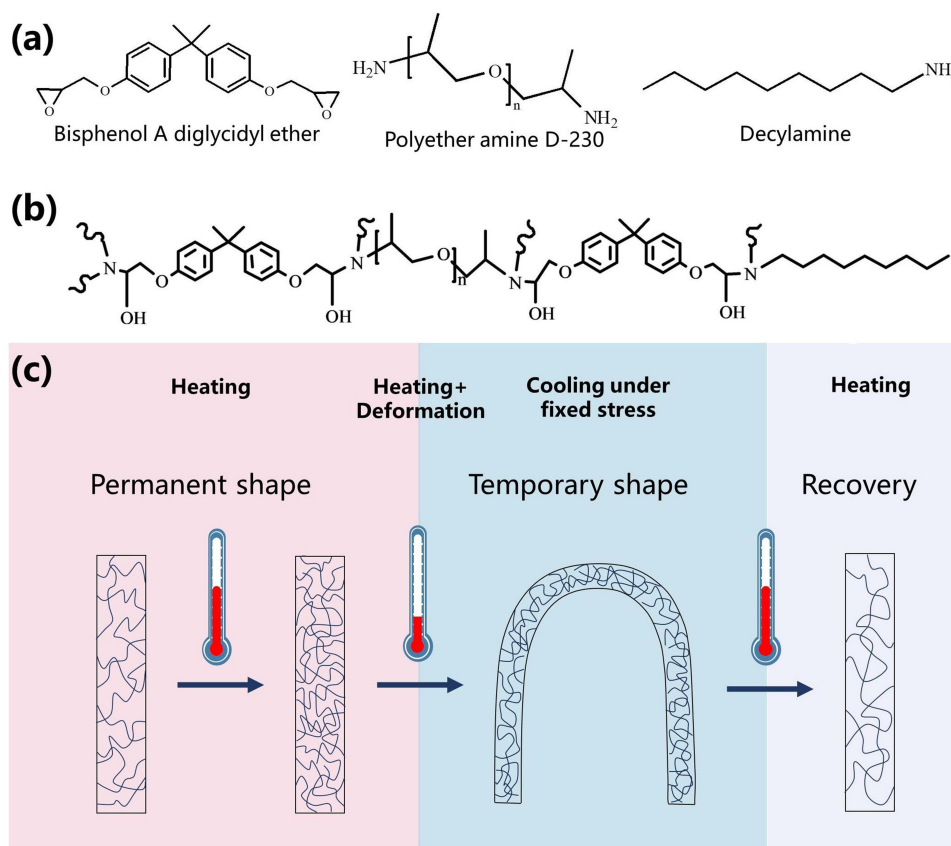
Figure 1 Schematic illustration of molecular structure and shape memory. (**a**) Chemical formula of bisphenol A diglycidyl ether; polyetheramine D-230; decylamine; (**b**) chemical formula of the shape memory polymer (SMPs), and (**c**) transition between the permanent and temporary shape of the SMPs.

Shape Memory Characteristic Tests

The shape memory effect is an important characteristic of SMPs, and SMPs with excellent shape memory effects have better prospects, so we tested the shape memory effect of SMPs and LSMPC to check whether it meets practice requirements.

In brief, both materials were molded into elongated strips and folded into a "U" shape at a temperature of 60 °C. They were held at this temperature for three minutes for measuring the fixed angle θ_{fixed} before being cooled down to room temperature. The folded specimens were then shaped back to their initial form via 45 °C warm water immersion or NIR light irradiation. The angle in the post-recovered site was then recorded as θ_{final}. The rates of shape fixation (R_f) and recovery (R_r) were determined using the following equations: $R_f = \theta_{fixed}/180° \times 100\%$ and $R_r = (\theta_{fixed} - \theta_{final})/\theta_{fixed} \times 100\%$.[27]

Mechanical Test

The compression properties of SMPs and LSMPC were tested according to GB/T 1041–2008, in which the size of the samples was $10 \times 10 \times 4$ mm, and the compression rate was 1 mm/min until the yielding platform appeared.

Thermodynamic Performance Tests

The glass transition temperatures of SMPs and LSMPC were determined using a differential scanning calorimeter (DSC, DSC-60Aplus, METTLER TOLEDO, Japan) in a nitrogen atmosphere. Samples were heated from 25 °C to 150 °C, held for 3 min, then cooled to −30 °C, held for 3 min to remove thermal effects, and then heated to 150°C, all at a temperature rise and fall rate of 10 °C/min during the process. For thermogravimetric analysis (TGA, TG/DTA6300, NSK Ltd., Japan), samples were heated from 25 °C to 700 °C in a nitrogen atmosphere at a rate of 10 °C/min. Dynamic mechanical testing (DMA, TA Q800, USA) was performed to determine the storage modulus and tan δ of the samples at different temperatures, the specimens were heated from 30 °C to 150 °C at a rate of 3 °C/min in tensile loading mode at a test frequency of 1 Hz.

In vitro Biocompatibility Tests

Mouse embryonic osteoblast precursor cells were used for cellular experiments to test the biocompatibility of LSMPC-0.5. Mouse osteoblastic MC3T3-E1 cells (Punosai Life Technology, China) were cultured at 37 °C in a humidified environment with 5% CO_2. A 1% penicillin–streptomycin mixture, and 10% fetal bovine serum were added to the α-MEM. The specimens were prepared as $10 \times 10 \times 1$ mm pieces, immersed in the 75% alcohol solution for 12 h for cleaning, and then soaked in hot water at 50 °C for five days to eliminate incompletely reacted small molecules. Subsequently, cellular experiments were conducted after one day of UV sterilization. Sterilized samples were initially moved to a 24-well plate, and cell suspensions with a density of 3×10^4 were seeded.

After 1- and 3-days of culture, specimens were washed 3 times with PBS, and then stained using a Live/dead cell double staining kit. In brief, 500 μL of the Live/Dead staining solutions were added to each well, incubated for 20 min away from light, washed twice with PBS, and then visualized using an inverted fluorescence microscope (CLSM, LEICA, Germany) to study the growth of MC3T3-E1 cells. On the other hand, the proliferation status of MC3T3-E1 cells was also quantitatively studied using a CCK-8 kit, coupled with an enzyme labeling instrument (Beijing Planck New Technology Co., Ltd., China) reading at 450 nm wavelength.

In vivo Biocompatibility Test

Subcutaneous Implantation in Rats

The animals used in this study were male SD rats, weighing 240 ± 10 g. The animal experiments of this study were approved by the Biomedical Ethics Committee of Hebei University Technology (HEBUTaCUC2022001). Our experimental protocols were conducted in accordance with the guidelines of the Association for Assessment and Accreditation of Laboratory Animal Care. The implants used were discs (10 mm in diameter and 0.5 mm thick), which were illuminated under UV light for 1 day to sterilize and disinfect them. Before implantation, the rats were anesthetized by intraperitoneal injection of chloral hydrate, the hair on the back was shaved, and the skin was wiped with iodophor

solution. A 12 mm incision was made on each side of the back with a scalpel, and the material was implanted subcutaneously and the wound was finally sutured.

Acute Toxicity Test
Blood was taken from rats one day after implantation of LSMPC-0.5, and blood routine tests were performed and compared with blood from rats without any treatment.

Histological Staining
After 14 days, the animals were euthanized and dissected to obtain skin tissue in contact with the implanted material fixed in a 10% paraformaldehyde solution. Tissue sections (5 μm) were processed with hematoxylin and eosin (H&E) or Masson staining, followed by light microscopy observation.

Integration of Cage-LSMPC and CSC
Preparation of Cage-LSMPC
LSMPC-0.5 solution was prepared by mixing 3 mL of bisphenol A diglycidyl ether, 366 μL of polyetheramine D-230, 1.5 mL of decylamine and 0.0261 g of Fe_3O_4, which was poured into a 3D printed mold and subjected to the same curing procedure as described above. The final size of the Cage-LSMPC was $40 \times 22 \times 10$ mm, where the wall thickness was 3 mm; then, the size of the center empty area was $34 \times 16 \times 10$ mm.

Shape Memory Characteristic Tests
The Cage-LSMPC was immersed in 60 °C hot water and compressed along its longitudinal axis to generate a temporary form. Subsequently, it was placed at room temperature for shape fixation, and then irradiated with a NIR laser (Changchun New Industry Optoelectronics Co., Ltd., China) to observe the shape recovery process.

Preparation of CSC
CSC consisted of $BaSO_4$, waxy starch and CPC, in which starch is used as a polymer to increase the homogeneity and injectability of the cement, and $BaSO_4$ is used to enhance the developability. The CPC was used as prepared according to previous reports.[28,29] α-TCP was mixed with $CaHPO_4 \, 2H_2O$ (DCPD) at a mass ratio of 9:1, and then ball-milled with ethanol (weight ratio of CPC: onyx balls: ethanol is 4:30:9) on a planetary ball miller (Changsha Miqi Instrument Co., Ltd., China) at 464 rpm for 6 h. After ball-milling, the CPC slurry was dried at 80 °C, milled into a powder, and stored in a vacuum desiccator for further study. $BaSO_4$, waxy starch and CPC were mixed thoroughly at a mass ratio of 1:1:3, and then added to 0.25 M Na_2HPO_4 solution with a liquid-solid ratio of 0.4 mL/g. The mixture was stirred thoroughly until homogeneous to form a self-coagulating viscous paste that could be solidified at room temperature and used as a filler material for cage.

Injectability Test
Glass slides were positioned on the top and bottom of the fusion apparatus to form an isolated environment mimicking the physiological structure of the vertebra. CSC was injected into the interior of the fusion cage via an injection channel. The flow of CSC into the fusion cage was evaluated visually, and the resulting CSC filled cage was labeled as Cage-LSPMC-cement.

Mechanical Tests
The compressive strength of Cage-LSMPC and Cage-LSMPC-cement were assessed using a universal testing machine (Meters Industrial Systems Ltd., China). The cage was compressed steadily at a 2 mm/min rate until a yield plateau was observed.[30]

Cyclic compression testing of the Cage-LSMPC and Cage-LSMPC-cement was carried out on a universal testing machine (Meters Industrial Systems Ltd., China) with force values between 140 and 280 N at a rate setting of 100 N/S for 1000 cycles.[31]

Statistical Analysis
Student's t-tests were used for statistical analysis to determine the statistical difference between the two groups. The results were expressed as mean ± standard deviation (SD). $p \leq 0.05$ was considered statistically significant.

Results and Discussion

Photothermal and Shape Memory Characteristics of SMP and LSMPC

SMPs are highlighted by its ability to return from a fixed temporary shape to a permanent shape when subjected to external stimulation. Typically, thermal stimulation is employed to induce this shape transition. When the external temperature reaches the transition temperature, the molecular chains of SMP are activated from a glassy state to an elastic state, which is critical for the material to accomplish shape changes under the impact of external forces. As illustrated in Figure 1c, the molecular chains freeze and retain the temporary shape as the temperature falls below the transition temperature. Only when the external temperature rises above the transition temperature again, can the molecular chains revert to their initial state due to entropic elasticity.

In this study, SMPs incorporated with different quantities of photothermal Fe_3O_4 nanoparticles were fabricated to explore the remote control of material shape through NIR irradiation. Figure 2a displays the heating curves from the different LSMPCs under NIR light irradiation at 1 W. After 2 min of irradiation, LSMPC-0.3, LSMPC-0.5, and LSMPC-0.8 reached approximately 45, 62, and 80 °C, respectively. The increase in LSMPC temperature is attributed to the photoluminescence[32] of Fe_3O_4 and correlates with content. In contrast, no such photothermal phenomenon was found for the SMPs alone. Therefore, photothermal Fe_3O_4, which converts light energy into heat energy under NIR, was utilized as a "switch" for the remote control of the SMP shape recovery.

The shape memory repeatability of SMP and LSMPC was tested over 20 cycles in 45 °C water. The results showed that within 20 cycles, SMPs and LSMPC materials exhibited shape recovery ratios exceeding 90%, revealed excellent shape memory characteristics (Figure 2b). Regarding the photothermal responsiveness and the shape memory characteristic, LSMPC-0.5 was selected for subsequent experiments.

To visualize the shape memory process, both SMPs and LSMPC-0.5 sticks were pre-warmed in water at 60 °C and then subjected to an external force and folded into a "U" shape. After cooling down to room temperature, their temporary shapes were stabilized. When exposed to 60 °C aqueous environment again, both materials recovered to their original states (Figure 2c and d). However, when the "U"-shaped SMPs and LSMPC-0.5 were exposed to NIR light irradiation, only the LSMPC-0.5 recovered back to its original shape (Figure 2e). Figure 2f illustrates the complete process of shape recovery, fixation, and restoration for LSMPC-0.5. The sensitivity of LSMPC-0.5 to NIR light played the crucial role in precise on-site control of its shape change.

Thermodynamic Performance Analysis

The thermal properties of SMPs and LSMPC-0.5 were evaluated through differential scanning calorimetry (DSC) to determine their glass transition temperatures (T_g). The T_g values for SMPs and LSMPC-0.5 were found to be around 43 °C (Figure 3a), suggesting that the addition of Fe_3O_4 had minimal impact on T_g. The transition temperature was confirmed to be slightly above the body temperature, capable of avoiding interference by body temperature. In addition, thermogravimetric analysis (TGA) curves revealed that the initial decomposition temperature of SMPs was 345 °C, whereas LSMPC-0.5 exhibited a reduced initial decomposition temperature of 335 °C, along with a decrease in the temperature of the maximum weight loss rate from 374 °C to 364 °C (Figure 3b). This change was attributed to the accelerated heat transfer fact within polymer matrix induced by Fe_3O_4.[33]

Furthermore, mechanical testing showed the compression modulus of SMPs and LSMPC-0.5 were 389 MPa and 386 MPa, respectively. The limited compressive modulus difference was attributed to the poor interfacial interaction between Fe_3O_4 and SMPs (Figure 3c and d).[34] Figure 3e and f depict the storage modulus and tan δ of SMPs and LSMPC-0.5, respectively. The storage modulus of the composites exceeded 1200 MPa at a temperature of 44 °C, indicating the ability to maintain structural stiffness and provide a large elastic recovery during the shape transformation process.[35] This characteristic could prevent the failure of the materials to return to their original shape when subjected to an external force. In addition, the temperature corresponding to the peak of tan δ also indicated that the introduction of Fe_3O_4 had essentially no effect on the transition temperature of LSMPC.
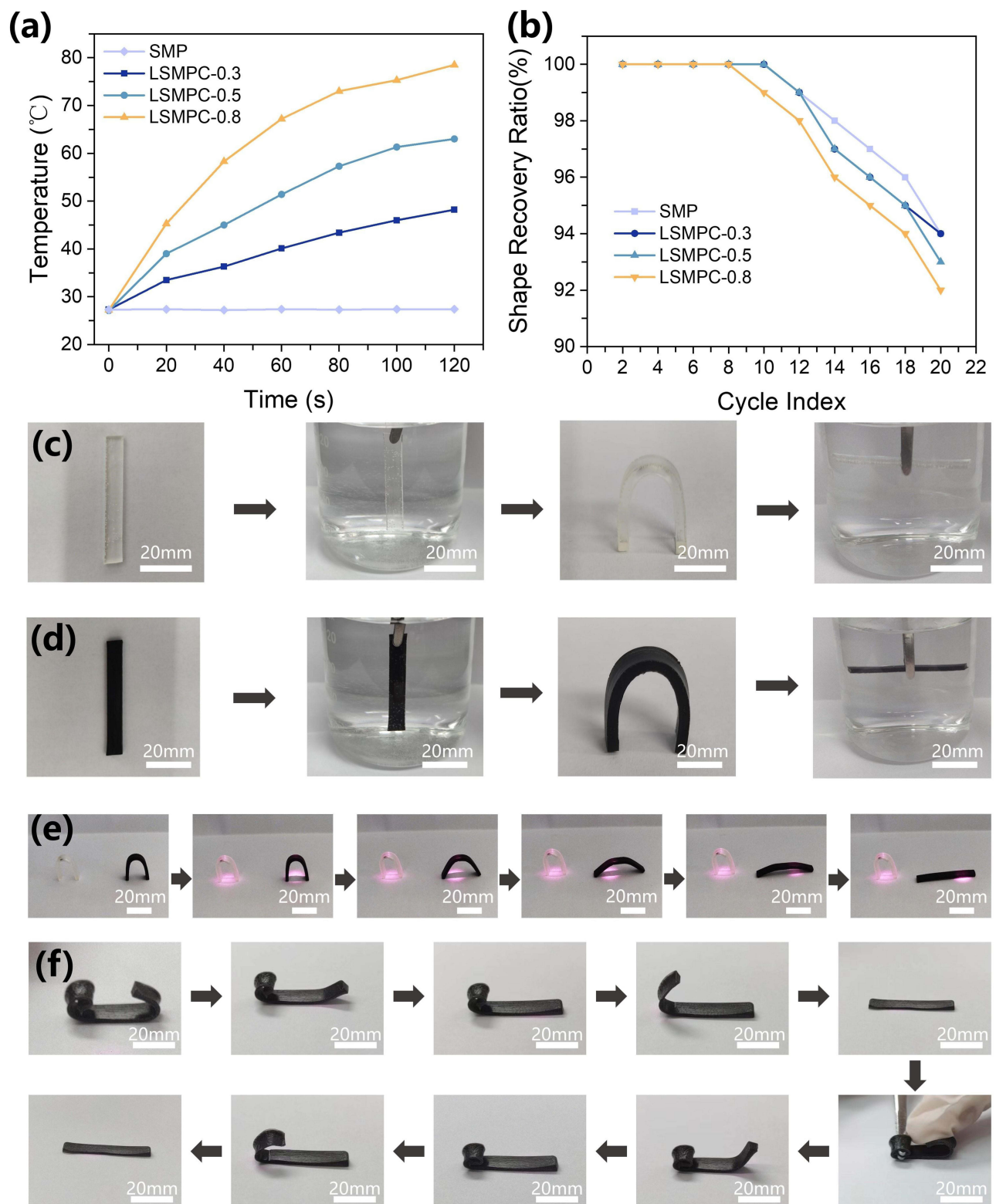
Figure 2 Temperature-sensitive and NIR-sensitive shape memory. (**a**) heating curve under near infrared laser irradiation (1W, 20 cm); (**b**) 20 times deformation recovery ratio, shape fixation and shape recovery behavior in hot water: (**c**) SMPs; (**d**) LSMPC-0.5; (**e**) deformation behavior of SMPs and LSMPC-0.5 under near infrared laser irradiation (pink shows the NIR light reflection on the table), (**f**) LSMPC-0.5 programming process: shape recovery-fixed-recovery.
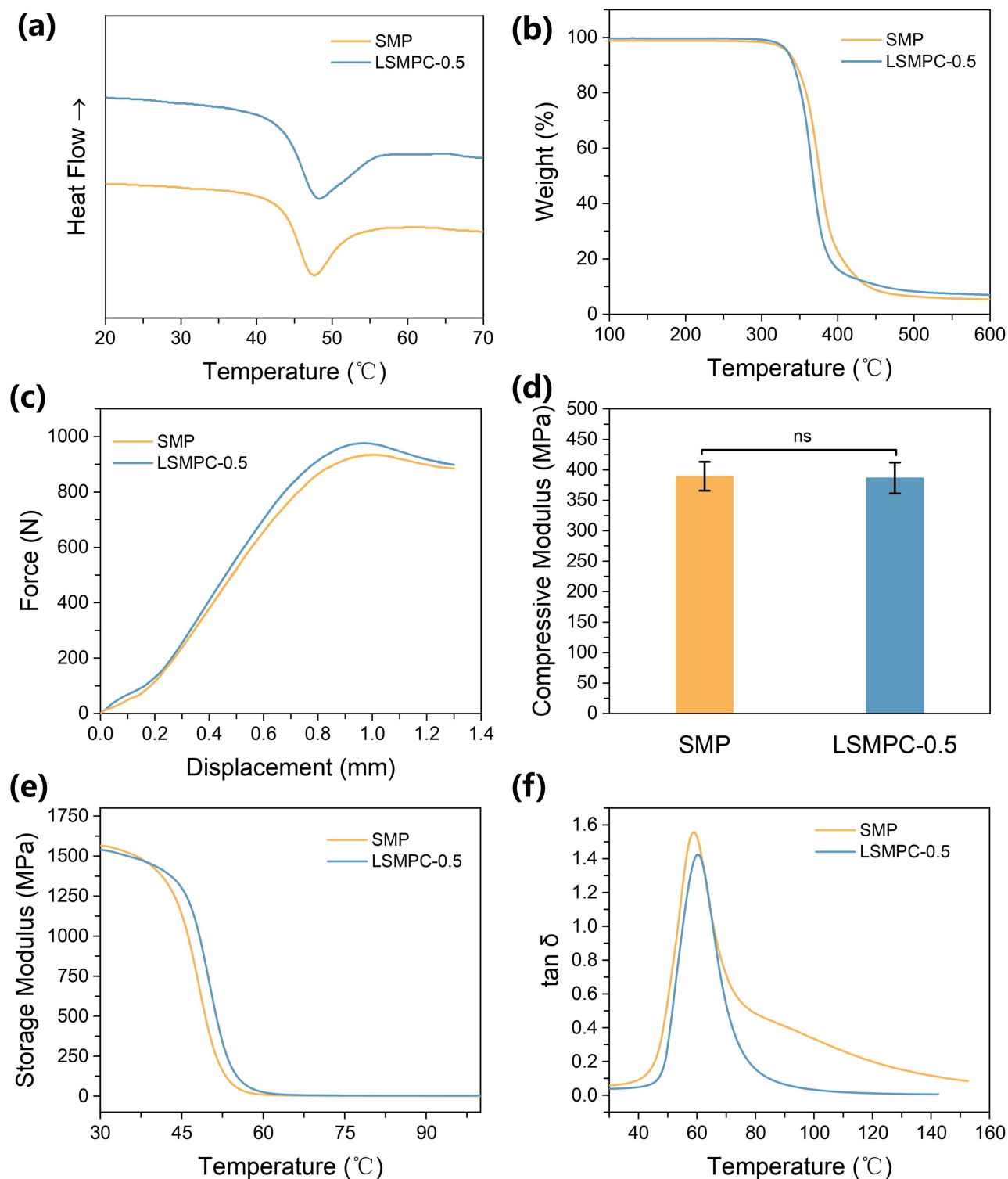
Figure 3 Thermodynamic properties. (**a**) DSC curve; (**b**) TGA curve; (**c**) force–displacement curve; (**d**) compressive modulus (ns, no significant difference); (**e**) storage modulus; and (**f**) tan δ curve of SMPs and LSMPC-0.5.

In vitro Cytocompatibility Properties

It was found that during LSMPC preparation, toxic monomers such as decylamine could not be fully consumed. To minimize the toxicity, the molded device required post-treatment steps such as soaking in alcohol and hot water. To assess the material's biocompatibility, we utilized the CCK-8 method to investigate MC3T3-E1 cell density on the

material surface at different culture durations. As shown in Figure 4a, cells could proliferate well on the surface of the material and no difference was found between test group and the control (Glass) at days 1 and 3. Cell adhesion and proliferation on the material surface were assessed using live-dead fluorescence staining, indicating no significant difference from the control as well (Figure 4b-g).

In vivo Histocompatibility

Figure 5a depicts the process of subcutaneous implantation of LSMPC-0.5 in rats. Compared with day 0, the implantation site at day 14 was essentially repaired with no obvious surgical traces such as infection or bulging, demonstrating in vivo biocompatibility (Figure 5b and c). H&E and Masson staining results were used to observe the inflammatory response of the samples after implantation. As shown in Figure 5d and e, no inflammatory cell infiltration was detected, indicating no significant inflammatory response. Dense connective tissue and well-aligned fibrous tissue were observed, indicating that LSMPC-0.5 has good histocompatibility. Acute toxicity experiments also showed no significant difference in blood counts between rats implanted with LSMPC-0.5 and rats without any treatment (Table 1).

Preparation and Structure of Cage-LSMPC

The preparation of the interbody fusion cage, its schematic and actual images are shown in Figure 6. According to the diagram, the mixture was poured into a pre-customized silicone mold to generate cage. The final Cage-LSMPC was easily achieved through a demolding procedure after curing. Before implantation, the shape of Cage-LSMPC was altered to reduce its size. After implantation, it was irradiated with NIR light to restore its original shape. Figure 6b shows the structure of the Cage-LSMPC designed according to the fusion device currently applied in lumbar spinal fusion surgery. An overall size of $40 \times 22 \times 10$ mm was used, along with a wall thickness designed to be 3 mm. In addition, an injection hole with a diameter of 4 mm was designed on one side to serve as a delivery channel for the CSC. This size could be altered based on practice requirement. The change in the size of the Cage-LSMPC is depicted in Figure 6c. The original width of the fusion cage was 21.67 mm. After altering its shape, the width was reduced to 8.8 mm, which is 2/5th the size of the original, paving the possibility to reduce surgical incision size in practice.

In vitro Feasibility Study

Figure 7a displays the shape recovery process of the cage under NIR light irradiation. It took 5 min to accomplish the shape recovery transition. Previous research reported that it can cause damage to tissues when the temperature is over 45 °C for a long period.[36] Although the transformation temperature of the prepared LSMPC is about 45 °C, the shape recovery can be completed within 5 minutes, indicating limited thermal damage to human tissues.
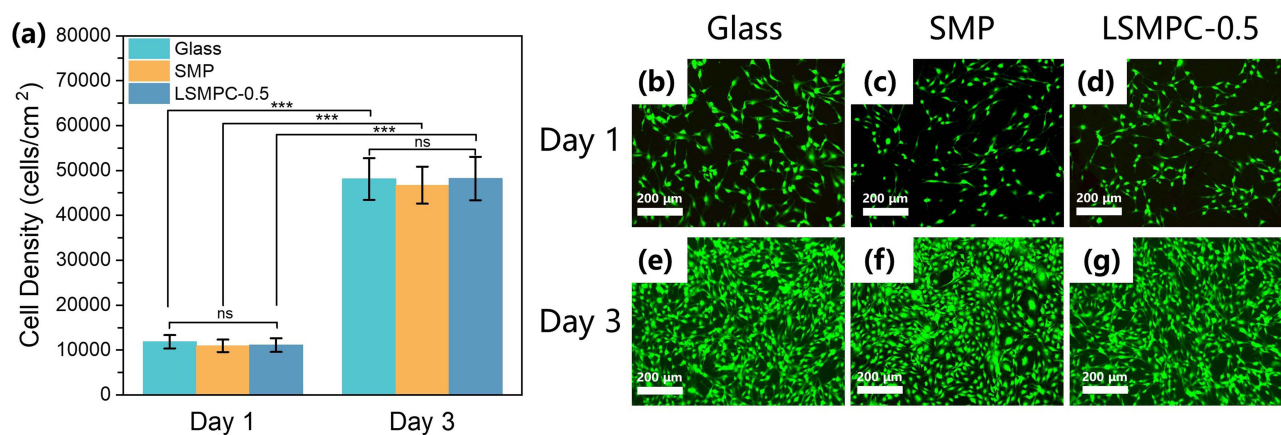
Figure 4 Cytocompatibility. MC3T3 cells cultured on the SMPs materials for 1 and 3 days: (**a**) cell density (ns, no significant difference; ***$p<0.001$); (**b–g**) Merged fluorescent images.
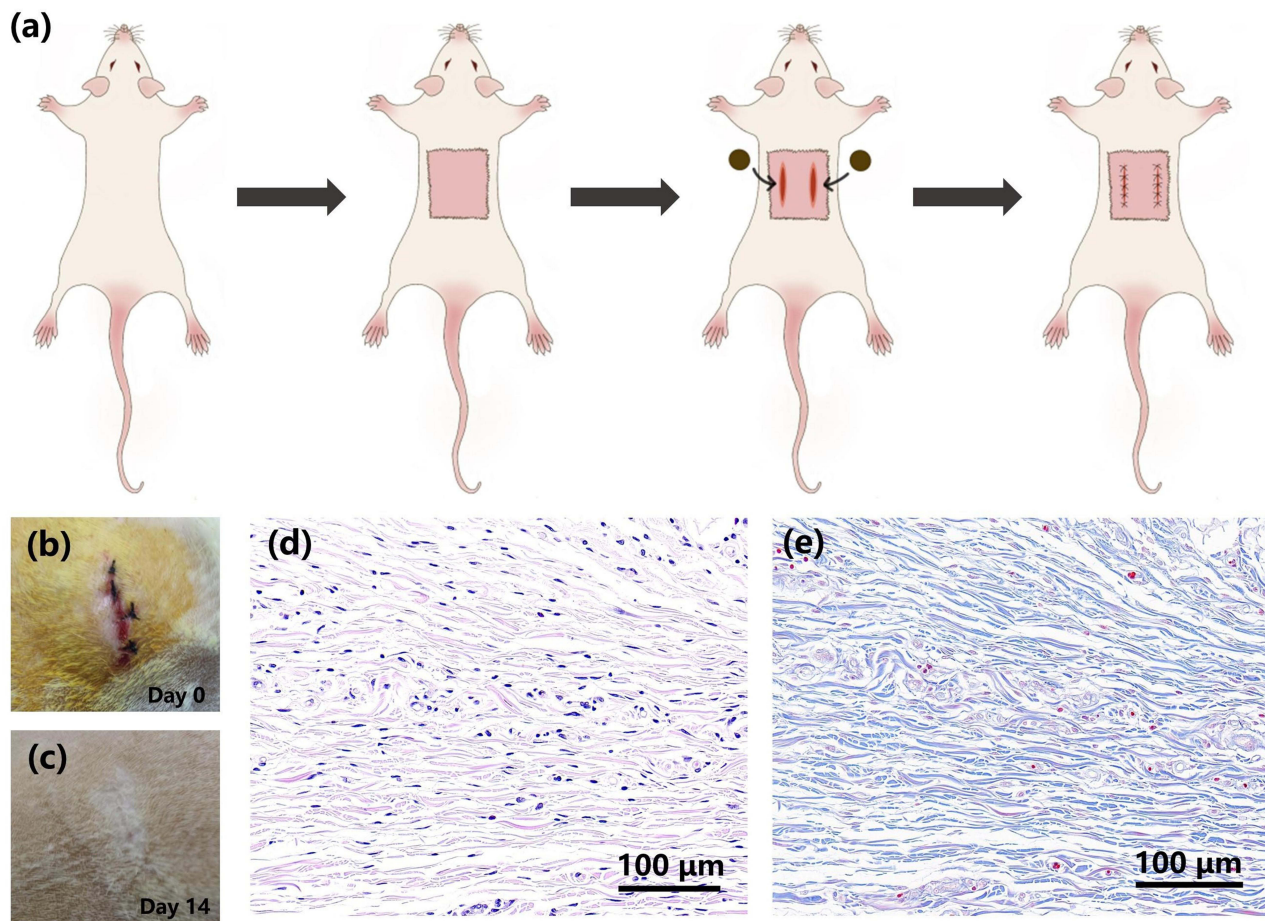
Figure 5 In vivo histocompatibility of SMPs in rats. (**a**) Schematic illustration of subcutaneous implantation experiment in rats, (**b**, **c**) images of wound appearance at day 0 and 14 of subcutaneous implantation in rats, histological analysis of LSMPC-0.5 after subcutaneous implantation for 14 days: (**d**) HE staining; and (**e**) Masson trichrome staining.

Figure 7b depicts the schematic diagram of the cage pre- and post-deformation in the model, illustrating the expansion of the folded cage in the interbody space to provide mechanical stabilization for the segments. The process of injecting bone cement into the fusion device is illustrated in Figure 7c. The CSC utilized in this study was developed by our research team specifically for kyphoplasty.[29,37] It is non-exothermic, non-leaky, and superior in terms of

Table 1 Blood Routine Examination Result

	Control	LSMPC-0.5
WBC (10^9/L)	10.50±1.25	15.57±4.15 (ns)
RBC (10^{12}/L)	6.28±0.27	6.24±0.47 (ns)
HGB (g/L)	139.33±4.51	136.33±12.34 (ns)
PLT (10^9/L)	1338.67±100.08	1071.00±302.13 (ns)
HCT (%)	43.70±0.70	42.70±3.02 (ns)
MCV (fL)	69.70±1.97	68.60±1.01 (ns)
MCH (pg)	22.17±0.86	21.80±0.66 (ns)

(Continued)

Table 1 (Continued).

	Control	**LSMPC-0.5**
MCHC (g/L)	318.33±8.96	318.33±6.66 (ns)
MPV (fL)	5.90±0.35	6.30±0.10 (ns)

Abbreviations: WBC, White blood cell; RBC, Red blood cell; HGB, Hemoglobin; PLT, Platelets; HCT, Hematocrit; MCV, Mean corpuscular volume; MCH, Mean corpuscular hemoglobin; MCHC, Mean corpuscular hemoglobin concentration; MPV, Mean platelet volume.

mechanical suitability, osseointegration, bioactivity, and degradation as compared to traditional PMMA bone cement. Additionally, this CSC exhibits superior injectability, compressive strength, and visualization properties compared to other calcium phosphate-based bone cements. Prior to the injection operation, the fusion device was covered with a glass
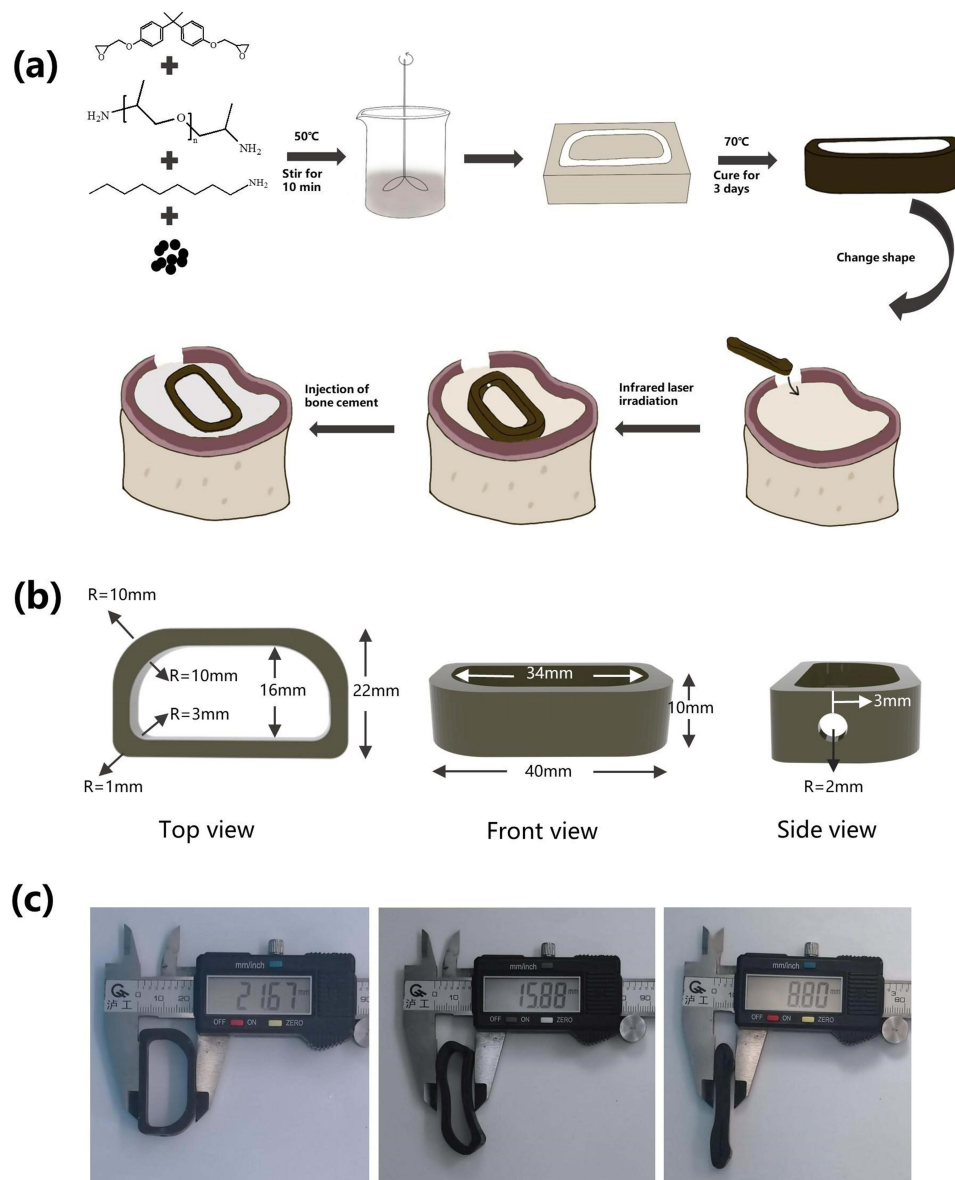
Figure 6 Design and fabrication of Cage-LSMPC. (**a**) Preparation and application process of Cage-LSMPC, (**b**) schematic of the three-dimensional structure of Cage-LSMPC, and (**c**) size of Cage-LSMPC before and after deformation.
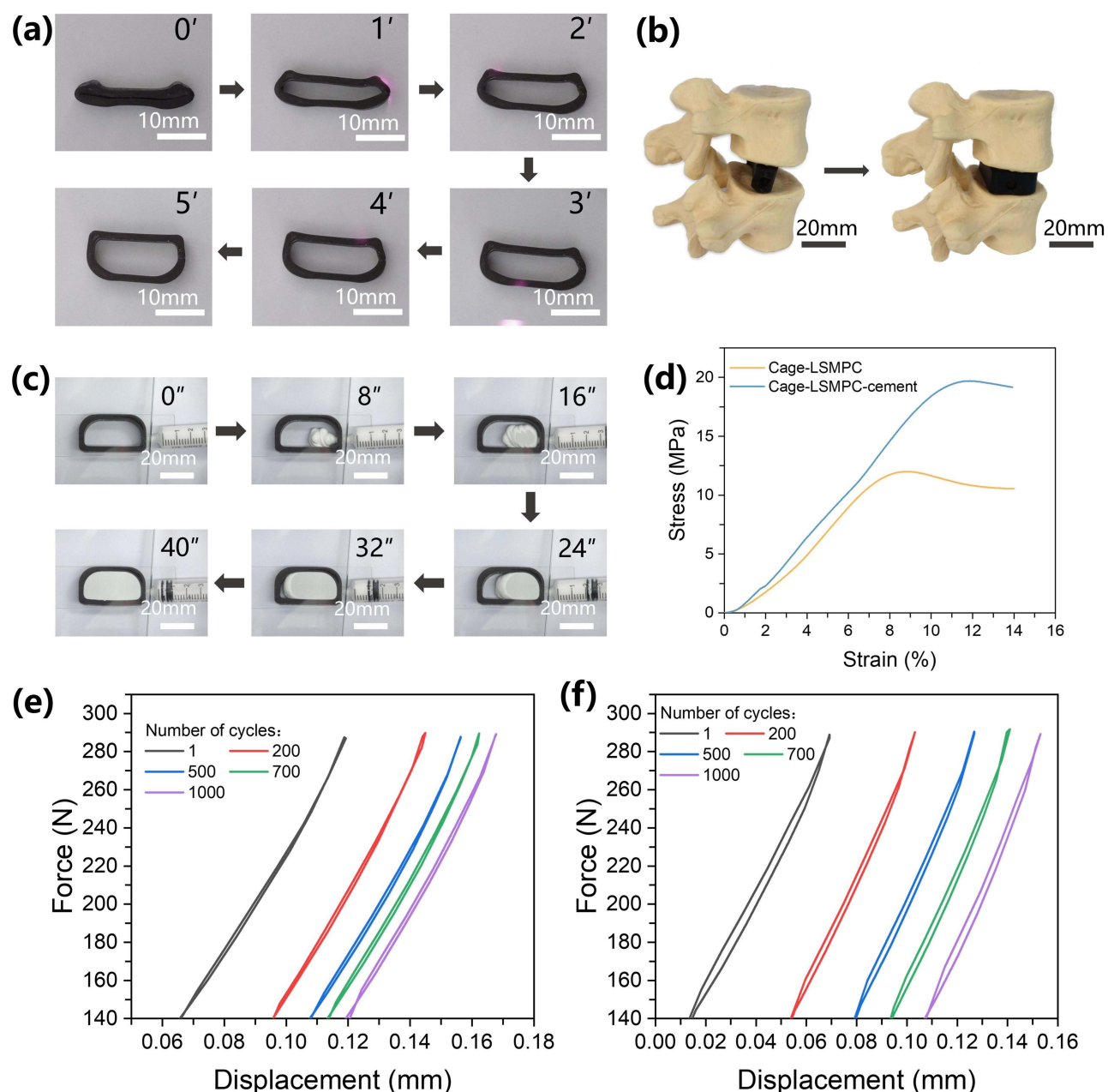
Figure 7 Feasibility of spinal fusion device. (**a**) Shape recovery process of Cage-LSMPC under NIR light irradiation (pink reflection shows the NIR light), (**b**) demonstration of the Cage-LSPMC shape change in the model before and after shape change, (**c**) the process of injecting bone cement into the Cage-LSMPC, (**d**) stress–strain curve of Cage-LSMPC and Cage-LSMPC-cement, cyclical fatigue test of the (**e**) Cage-LSMPC and (**f**) Cage-LSMPC-cement.

sheet to mimic the adjacent vertebrae to the disc. During the injection, it took 40 seconds for the CSC to diffuse homogeneously throughout the internal space of the fusion device to completely fill the space of cage.

Figure 7d illustrates the mechanical properties of the fusion device with and without the presence of bone cement. The results showed that the strength of Cage prepared from LSMPC was lower than the current Cage prepared with different shape structures of PEEK (several tens of MPa)[38] and Ti (several hundreds of MPa),[39] which was only 12 MPa. In contrast, the strength of the final CSC-filled cage was elevated to 20 MPa, which is 4.3 times of the minimal strength of male lumbar vertebrae, and the modulus was also increased from 168 MPa to 198 MPa, which is 3.3 times the modulus of the male lumbar spine.[40] The slightly higher modulus and sufficient strength enabled long-term use in the absence of stress barriers. As shown in Figure 7e and f, the cyclic fatigue test results show that the height drop was less

than 0.2 mm after 1000 cycles, only 2.0% of the original specimen size. This observation demonstrated the long-term durability of the Cage under physiological load conditions. As such, the Cage-LSMPC can be used as a basic platform to act as a "carrier" for the bone cement, which can be simultaneously mixed with bioactive factors or drugs to promote osteogenesis and improve fusion rates.

It has been shown in the literature that minimally invasive interbody fusion has a 40% lower complication rate compared to conventional interbody fusion,[41] implying the potential advantages of the prepared Cage-LSMPC in reducing the surgical incision, providing a quicker postoperative recovery, and reducing the risk of surgical infection. Degradation experiments were performed on LSMPC-0.5 for 7 days. The mass of LSMPC-0.5 did not change within 7 days (Supplementary Figure 1), indicating the non-degradability of LSMPC-0.5. We have reported that CSC degraded by 12% after 8 weeks,[36] which would provide space for new bone growth and osseointegration. Narrow facet interbody fusion devices currently used in minimally invasive interbody fusion are prone to interbody stress shielding, leading to vertebral collapse and fusion failure.[42,43] Whereas the Cage-LSMPC can return to its original shape after being delivered through the surgical working cannula, providing sufficiently sized fusion device for lumbar spine. The large size of the interbody fusion can better stabilize the vertebral body, avoiding interbody collapse and secondary surgery.

Conclusion

Here, we designed and fabricated a very promising spinal fusion device for minimally invasive surgery with reduced incision size for implantation. Compared to current fusion devices prepared with Ti and PEEK materials, the fabricated Cage-LSMPC integrates NIR light-controlled shape memory function, allowing the design of a temporary shape with a size 2/5th of the original shape. After implantation, the original shape could be restored within just 5 min by remote NIR light control. In vitro cytotoxicity and in vivo rat subcutaneous implantation experiments showed that the device had good biocompatibility. These characteristics thereby could effectively minimize the surgical incision during implantation, reducing the risk of bleeding and tissue damage, and overall improve medical outcomes post-surgery. In addition, the minimally invasive filling of injectable bone cement CSC is supposed to reinforce the mechanical stability in situ and accelerate bony fusion. All of these results collectively demonstrated that the as-fabricated shape memory spinal fusion device has strong potential for use in minimally invasive lumbar fusion surgery.

Acknowledgments

Disclosure

The authors report no conflicts of interest in this work.

References

1. Laubach M, Kobbe P, Hutmacher DW. Biodegradable interbody cages for lumbar spine fusion: current concepts and future directions. *Biomaterials*. 2022;288:121699. doi:10.1016/j.biomaterials.2022.121699
2. Cruz A, Ropper AE, Xu DS, et al. Failure in Lumbar Spinal Fusion and Current Management Modalities. *Seminars Plastic Surgery*. 2021;35 (1):54–62. doi:10.1055/s-0041-1726102
3. Smorgick Y, Baker KC, Bachison CC, Herkowitz HN, Montgomery DM, Fischgrund JS. Hidden blood loss during posterior spine fusion surgery. *Spine J*. 2013;13(8):877–881. doi:10.1016/j.spinee.2013.02.008
4. Elgafy H, Bransford RJ, McGuire RA, Dettori JR, Fischer D. Blood loss in major spine surgery: are there effective measures to decrease massive hemorrhage in major spine fusion surgery? *Spine*. 2010;35(9 Suppl):S47–56. doi:10.1097/BRS.0b013e3181d833f6
5. Delaey J, Dubruel P, Van Vlierberghe S. Shape-Memory Polymers for Biomedical Applications. *Adv Funct Mater*. 2020;30(44):1909047. doi:10.1002/adfm.201909047

6. Wang L, Zhang F, Liu Y, Leng J. Shape Memory Polymer Fibers: materials, Structures, and Applications. *Adv Fiber Mater*. 2022;4(1):5–23. doi:10.1007/s42765-021-00073-z

7. Lendlein A, Gould OEC. Reprogrammable recovery and actuation behaviour of shape-memory polymers. *Nat Rev Mater*. 2019;4(2):116–133. doi:10.1038/s41578-018-0078-8

8. Chen X, Tan P, Wen Y, et al. Facile scalable one-step wet-spinning of surgical sutures with shape memory function and antibacterial activity for wound healing. *Chin Chem Lett*. 2020;31(6):1499–1503. doi:10.1016/j.cclet.2019.11.006

9. Zhou W, Tan P, Chen X, et al. Berberine-Incorporated Shape Memory Fiber Applied as a Novel Surgical Suture. *Front Pharmacol*. 2020:10. doi:10.3389/fphar.2019.01506

10. Lin C, Liu L, Liu Y, Leng J. 4D printing of shape memory polybutylene succinate/polylactic acid (PBS/PLA) and its potential applications. *Compos Struct*. 2022;279:114729. doi:10.1016/j.compstruct.2021.114729

11. Zhang C, Cai D, Liao P, et al. 4D Printing of shape-memory polymeric scaffolds for adaptive biomedical implantation. *Acta Biomater*. 2021;122:101–110. doi:10.1016/j.actbio.2020.12.042

12. Zhang Q, Zhao Z, Wu D, Chen K, Weng S. Mechanics-guided design of inflatable heterogeneous shape memory polymer vascular stents. *Int J Mech Sci*. 2023;254:108405. doi:10.1016/j.ijmecsci.2023.108405

13. Chen Y, Garces IT, Tang T, Ayranci C. Cellulose nanocrystals reinforced shape memory polymer cardiovascular stent. *Rapid Prototyp J*. 2021;27(1):37–44. doi:10.1108/RPJ-01-2020-0019

14. Chen L, Li W, Liu Y, Leng J. Nanocomposites of epoxy-based shape memory polymer and thermally reduced graphite oxide: mechanical, thermal and shape memory characterizations. *Compos Part B*. 2016;91:75–82. doi:10.1016/j.compositesb.2016.01.019

15. Wang Y, Cui H, Wang Y, et al. 4D Printed Cardiac Construct with Aligned Myofibers and Adjustable Curvature for Myocardial Regeneration. *ACS Appl Mater Interfaces*. 2021;13(11):12746–12758. doi:10.1021/acsami.0c17610

16. Miao S, Cui H, Esworthy T, et al. 4D Self-Morphing Culture Substrate for Modulating Cell Differentiation. *Adv Sci*. 2020;7(6):1902403. doi:10.1002/advs.201902403

17. Wang C, Yue H, Liu J, et al. Advanced reconfigurable scaffolds fabricated by 4D printing for treating critical-size bone defects of irregular shapes. *Biofabrication*. 2020;12(4):045025. doi:10.1088/1758-5090/abab5b

18. Xie H, Shao J, Ma Y, et al. Biodegradable near-infrared-photoresponsive shape memory implants based on black phosphorus nanofillers. *Biomaterials*. 2018;164:11–21. doi:10.1016/j.biomaterials.2018.02.040

19. Dai S, Yue S, Ning Z, Jiang N, Gan Z. Polydopamine Nanoparticle-Reinforced Near-Infrared Light-Triggered Shape Memory Polycaprolactone–Polydopamine Polyurethane for Biomedical Implant Applications. *ACS Appl Mater Interfaces*. 2022;14(12):14668–14676. doi:10.1021/acsami.2c03172

20. Yan N, Zheng Z, Liu Y, et al. Photo-responsive shape memory polymer composites enabled by doping with biomass-derived carbon nanomaterials. *Nano Res*. 2022;15(2):1383–1392. doi:10.1007/s12274-021-3674-7

21. Vakil AU, Ramezani M, Monroe MBB. Magnetically Actuated Shape Memory Polymers for On-Demand Drug Delivery. *Materials*. 2022;15(20):7279. doi:10.3390/ma15207279

22. Cui H, Miao S, Esworthy T, et al. A novel near-infrared light responsive 4D printed nanoarchitecture with dynamically and remotely controllable transformation. *Nano Res*. 2019;12:1381–1388. doi:10.1007/s12274-019-2340-9

23. Hampel GA, Yilmaz E, Massrey C, et al. History of Bone Grafts in Spine Surgery. *Cureus*. 2022;14(5):e24655. doi:10.7759/cureus.24655

24. Gruskay JA, Basques BA, Bohl DD, Webb ML, Grauer JN. Short-term adverse events, length of stay, and readmission after iliac crest bone graft for spinal fusion. *Spine*. 2014;39(20):1718–1724. doi:10.1097/brs.0000000000000476

25. Carragee EJ, Hurwitz EL, Weiner BK. A critical review of recombinant human bone morphogenetic protein-2 trials in spinal surgery: emerging safety concerns and lessons learned. *Spine j*. 2011;11(6):471–491. doi:10.1016/j.spinee.2011.04.023

26. Sun H, Liu C, Li X, et al. A novel calcium phosphate–based nanocomposite for the augmentation of cement-injectable cannulated pedicle screws fixation: a cadaver and biomechanical study. *J Orthop Translat*. 2020;20:56–66. doi:10.1016/j.jot.2019.08.001

27. Lin C, Lv J, Li Y, et al. 4D-Printed Biodegradable and Remotely Controllable Shape Memory Occlusion Devices. *Adv Funct Mater*. 2019;29(51):1906569. doi:10.1002/adfm.201906569

28. Liu H, Zhang Z, Gao C, et al. Enhancing effects of radiopaque agent BaSO4 on mechanical and biocompatibility properties of injectable calcium phosphate composite cement. *Mater Sci Eng C*. 2020;116:110904. doi:10.1016/j.msec.2020.110904

29. Gao C, Liu H, Yang H, Yang L. Fabrication and Characterization of Injectable Calcium Phosphate-based Cements for Kyphoplasty. *Mater Technol*. 2015;30(sup8):B256–B263. doi:10.1080/10667857.2015.1104828

30. Jia C, Zhang Z, Cao S, et al. A biomimetic gradient porous cage with a micro-structure for enhancing mechanical properties and accelerating osseointegration in spinal fusion. *Bioact Mater*. 2023;23:234–246. doi:10.1016/j.bioactmat.2022.11.003

31. Volpe RH, Mistry D, Patel VV, Patel RR, Yakacki CM. Dynamically Crystalizing Liquid-Crystal Elastomers for an Expandable Endplate-Conforming Interbody Fusion Cage. *Adv Healthcare Mater*. 2020;9(1):1901136. doi:10.1002/adhm.201901136

32. Sadat ME, Kaveh Baghbador M, Dunn AW, et al. Photoluminescence and photothermal effect of Fe3O4 nanoparticles for medical imaging and therapy. *Appl Phys Lett*. 2014;105(9). doi:10.1063/1.4895133

33. Liu H, Wang F, Wu W, Dong X, Sang L. 4D printing of mechanically robust PLA/TPU/Fe3O4 magneto-responsive shape memory polymers for smart structures. *Compos Part B*. 2023;248:110382. doi:10.1016/j.compositesb.2022.110382

34. Yue C, Li M, Liu Y, et al. Three-dimensional printing of cellulose nanofibers reinforced PHB/PCL/Fe3O4 magneto-responsive shape memory polymer composites with excellent mechanical properties. *Addit Manuf*. 2021;46:102146. doi:10.1016/j.addma.2021.102146

35. Zhang F, Wang L, Zheng Z, Liu Y, Leng J. Magnetic programming of 4D printed shape memory composite structures. *Compos Part A*. 2019;125:105571. doi:10.1016/j.compositesa.2019.105571

36. Sun Z, Li T, Wu F, et al. Precise Synergistic Photothermal Therapy Guided by Accurate Temperature-Dependent NIR-II Fluorescence Imaging. *Adv Funct Mater*. 2024;34(14):2311622. doi:10.1002/adfm.202311622

37. Liu H, Liu B, Gao C, et al. Injectable, biomechanically robust, biodegradable and osseointegrative bone cement for percutaneous kyphoplasty and vertebroplasty. *Int Orthopaedics*. 2018;42(1):125–132. doi:10.1007/s00264-017-3674-0

38. Chen P, Su J, Wang H, et al. Mechanical properties and microstructure characteristics of lattice-surfaced PEEK cage fabricated by high-temperature laser powder bed fusion. *J Mater Sci Technol*. 2022;125:105–117. doi:10.1016/j.jmst.2022.03.009

39. Wang H, Wan Y, Li Q, et al. Multiscale design and biomechanical evaluation of porous spinal fusion cage to realize specified mechanical properties. *Bio-Des Manuf.* 2022;5(2):277–293. doi:10.1007/s42242-021-00162-3

40. Barba D, Alabort E, Reed RC. Synthetic bone: design by additive manufacturing. *Acta Biomater.* 2019;97:637–656. doi:10.1016/j.actbio.2019.07.049

41. Lee MJ, Mok J, Patel P. Transforaminal Lumbar Interbody Fusion: traditional Open Versus Minimally Invasive Techniques. *J Am Acad Orthop Surg.* 2018;26(4):124–131.

42. Phan K, Mobbs RJ. Evolution of Design of Interbody Cages for Anterior Lumbar Interbody Fusion. *Orthop Surg.* 2016;8(3):270–277. doi:10.1111/os.12259

43. Hawasli AH, Khalifeh JM, Chatrath A, Yarbrough CK, Ray WZ. Minimally invasive transforaminal lumbar interbody fusion with expandable versus static interbody devices: radiographic assessment of sagittal segmental and pelvic parameters. *Neurosurgical Focus FOC.* 2017;43(2):E10. doi:10.3171/2017.5.FOCUS17197